PII: S0032-3861(96)00774-4

Polymer Vol. 38 No. 9, pp. 2191–2200 1997

0032-3861/97/$17.00 + 0.00

Toughening PET by blending with a functionalized SEBS block copolymer

V. Tanrattanakul, A. Hiltner* and E. Baer
Department of Macromolecular Science and Center for Applied Polymer Research, Case Western Reserve University, Cleveland, OH 44106, USA

and W. G. Perkins and F. L. Massey
Polyester Technical Center, Shell Chemical Company, Akron, OH 44305, USA

and A. Moet
Department of Chemical and Petroleum Engineering, United Arab Emirate University, Al-Ain, U.A.E.
(Received 23 April 1996; revised 11 July 1996)

Toughened poly(ethylene terephthalate) (PET) was obtained by blending with 1–5 wt% of a triblock copolymer with styrene end blocks and a functionalized ethylene/butylene midblock. The midblock was grafted with 2 wt% maleic anhydride. The blends were characterized for melt viscosity, domain morphology, and tensile stress–strain behaviour at two strain rates. Blending increased the fracture strain of PET by more than a factor of 10. The fracture strain was affected to some extent by both blend composition and processing conditions. However, neither blend composition nor processing conditions strongly influenced the melt viscosity of the blend or the particle size in the blend. These observations are consistent with *in situ* formation of a graft copolymer by reaction of PET hydroxyl end groups with maleic anhydride. The graft copolymer acted as an emulsifier to decrease the interfacial tension and reduce the tendency of dispersed particles to coalesce, and promoted adhesion between the phases in the blend. Evidence for the presence of a graft copolymer was obtained by i.r. analysis of blend extracts. © 1997 Elsevier Science Ltd.

(Keywords: toughening; PET; SEBS)

INTRODUCTION

Although polar engineering thermoplastics such as polyamides, polyesters and polycarbonate are tough in an unnotched situation, they tend to be notch sensitive and stress concentrations can cause the fracture mode to change from ductile to brittle. Impact-modified versions of these thermoplastics have been developed by rubber-toughening without seriously compromising other properties. In the quest for tougher engineering thermoplastics, polycarbonate and polyamides, especially nylon 6,6 and nylon 6, have received more attention than polyesters. Furthermore, most of the studies of polyesters have focused on poly(butylene terephthalate) (PBT) rather than on PET. Although it is anticipated that the same general concepts of toughening apply, it is of interest to examine specifically the issues in toughening PET.

Blending polybutadiene or a conventional styrenic block copolymer with a polar thermoplastic is usually not effective for impact modification[1,2]. Blending yields neither the desired particle size nor the required degree of interfacial adhesion. As an approach to control both particle size and adhesion, the composite nature of core-shell rubbers is quite attractive. The rubbery core provides resistance to impact, whereas the grafted glassy shell provides rigidity for retention of particle size and shape over a wide range of processing conditions. Moreover, the composition of the shell can be chosen for good compatibility with the matrix to promote dispersion during processing and adhesion in the blend. This approach is particularly effective for toughening polycarbonate because of good compatibility of the poly(methyl methacrylate) shell with the matrix[3–5]. It is also possible to toughen PBT with a core-shell rubber, particularly if the blend also contains some polycarbonate to facilitate particle dispersion[6,7].

An alternative approach to impact modification of condensation polymers involves incorporation of reactive functional groups into the elastomer. The *in situ* graft copolymer formed by reaction with the thermoplastic matrix reduces interfacial tension to improve dispersion during processing, and improves adhesion of the rubber to the thermoplastic in the solid state. Because the rubber phase is broken up and dispersed during the blending operation, the effectiveness of the rubber modification depends on processing conditions[8,9]. Reactive processing approaches for toughening PBT have been demonstrated. Enhanced impact performance has been attributed to the graft copolymer produced by reaction of hydroxyl end groups of PBT with maleated ethylene–propylene rubber[9,10]. An alternative approach

* To whom correspondence should be addressed

involves reaction of a maleate-modified PBT fraction with an unsaturated rubber to form a graft copolymer[11].

Poly(ethylene terephthalate) is chemically and physically similar to PBT. A higher melting point, which provides a higher use temperature, and slower crystallization rate are the primary differences. Because the higher melting point requires a higher processing temperature, toughening systems commonly employed in PBT undergo thermal degradation at PET processing temperatures. An alternative chemistry for *in situ* formation of a PET graft copolymer involves reaction of PET terminal groups with epoxy groups of an elastomeric ethylene–ethyl acrylate–glycidyl methacrylate copolymer[12].

Numerous studies illustrate that addition of a maleated polystyrene–poly(ethylene-*co*-butylene)–polystyrene (SEBS) triblock copolymer improves the toughness of nylon 6,6 and nylon 6[13–16], and also polyamides with higher methylene content[17,18], presumably as a result of the graft copolymer formed by reaction of terminal amino groups with the maleic anhydride functionality. There is evidence that functionalized SEBS also improves the toughness of polyesters[1]. The level of functionalized elastomer required to change the fracture mode of polyamides or polyesters from brittle to ductile in an Izod impact test is typically 20%. In order to demonstrate the usefulness of functionalized SEBS for toughening PET, the influence of significantly lower elastomer levels on blend morphology and blend properties was studied. The notched Izod test is frequently employed to determine toughness because of its simplicity, convenience, and acceptance by the polymer community. It is also considered the most severe of the toughness tests. In the present study, a less severe method, unnotched tensile testing, was used to differentiate among materials[19].

EXPERIMENTAL

Materials

The PET provided by the Shell Chemical Company (Akron, OH) was Cleartuf® 7207, a bottle grade resin with an intrinsic viscosity of 0.72 dl g^{-1}, molecular weights $M_n = 24\,000$ and $M_w = 49\,000$, and hydroxyl number of 1.4 mol/mol. The PET was blended with small amounts of Kraton® FG1901X (SEBS-g-MA) provided by the Shell Chemical Company. The ratio of styrene to ethylene/butylene in the triblock copolymer was reported by the manufacturer to be 28/72 by wt% and the ethylene/butylene midblock was grafted with 2 wt% maleic anhydride. Alternatively, the PET was blended with Kraton® G1652, the unfunctionalized analogue of Kraton® FG1901X. The molecular weight of the SEBS-g-MA was determined by g.p.c. using the Varian DS-651 LC Star System with THF as the eluent. The styrene equivalent molecular weights were $M_n = 74\,000$ and $M_w = 77\,000$. These molecular weights were used to calculate an average concentration of 15 anhydride groups per polymer chain.

Processing

The PET was dried at 150°C for 15 h *in vacuo* and the SEBS-g-MA was dried at 80°C for 24 h *in vacuo* before blending. The pellets were dry blended in compositions of 1, 2 and 5% by weight SEBS-g-MA and extruded in a Haake Rheomex TW-100 twin screw extruder with partially intermeshing, counter-rotating, conical screws with converging axes. The average screw diameter was 25.4 mm and the average L/D ratio was 13/1. Two barrel temperatures (260 and 280°C) and two screw speeds (20 and 35 rpm) were used. The molten blends were extruded through a 3 mm die, quenched in water and pelletized. The pellets were dried *in vacuo* at 150°C for 15 h and stored in a desiccator.

The pellets were injection moulded into 3.18 mm type I tensile bars (ASTM D638) using a Battenfeld Unilog 4000 injection moulding machine. Typical operating conditions were 260°C barrel temperature, 265°C nozzle temperature, 25°C mould temperature, 1050 psi injection pressure, and 900 psi back pressure. The tensile bars were stored in a desiccator until tested.

Characterization

The intrinsic viscosity of PET, as received, in the extruded blends, and in the injection moulded blends, was measured at 25°C in an Ubbelohde-type viscometer using 60/40 w/w phenol/tetrachloroethane as the solvent. The SEBS-g-MA was filtered out and the concentration of the solution was normalized by the wt% of PET in the blend. The number average molecular weight (M_n) was determined according to[20]

$$[\eta] = 7.50 \times 10^{-4}(M_n)^{0.68} \quad (1)$$

Blends of PET with approximately 25 wt% of functionalized SEBS-g-MA or 25 wt% of unfunctionalized SEBS were prepared as described above using processing conditions of 280°C/35 rpm. The blends were extracted in a Soxhlet extractor with refluxing THF for 37 h. The THF-soluble fraction was precipitated in ethanol. The extraction was repeated with fresh THF for 13 h. No precipitate was obtained from the second extraction. Both the THF-soluble fraction and the THF-insoluble fraction were air dried for 24 h and dried *in vacuo* at 80°C for 24 h. The fractions were characterized by *FT*i.r. using the Nicolet 800 FTIR in the photoacoustic mode.

Extruded pellets were etched with THF at ambient temperature for 8 h, dried *in vacuo* at 100°C for 8 h, coated with 90 Å of gold and examined in the JEOL 840A scanning electron microscope. The sizes of 300–500 particles were measured with the Optimas image analysis software to obtain the average particle size and the size distribution. Injection moulded specimens were cryogenically fractured both parallel and perpendicular to the injection direction. These fracture surfaces were etched with THF and examined in the SEM.

Tensile tests were carried out in an Intron Model 1123 at ambient temperature using two crosshead speeds, 50 and 500 mm min^{-1}, which corresponded to strain rates of 100 and 1000% min^{-1}. The yield stress and elongation at break were obtained from the load–displacement curve. At least five specimens were tested for each condition.

All d.s.c. analyses were carried out in a Perkin Elmer 7 Series system with heating and cooling rates of 10°C min^{-1}. Specimens weighing 5–8 mg for d.s.c. analysis were cut from the centre of the injection moulded tensile bars and from the necked region of tensile-tested specimens. Percent crystallinity was based on a heat of fusion for PET of 122 J g^{-1} [21,22].

Melt rheology

The melt viscosity was measured in an Instron Model 3211 capillary rheometer. Test temperatures were 260 and 280°C, and the shear rate was varied from 13 to 1333 s^{-1}. Extruded pellets were dried at 100°C *in vacuo* overnight prior to testing. Approximately 25 g of sample was tamped into the rheometer barrel under a nitrogen blanket and preheated at the test temperature for 3 min. Extrusion was through a stainless steel capillary die, 25.4 mm long and 1.32 mm in diameter (L/D ratio of 19/2) having a 90° conical entrance angle. The Bagley and Rabinowitsch corrections were not made.

The Newtonian shear rate at the capillary wall ($\dot{\gamma}_w$) was calculated as a function of crosshead speed (v), plunger diameter (d_p), and capillary diameter (d_c) according to

$$\dot{\gamma}_w = \frac{2v(d_p)^2}{15(d_c)^3} \quad (2)$$

and the shear stress at the capillary wall (τ_w) was calculated as a function of the extrusion force or the force pushing the material through the capillary (F), the plunger diameter, the capillary diameter, and the capillary length (L_c) as

$$\tau_w = \frac{Fd_c}{\pi L_c (d_p)^2} \quad (3)$$

The apparent viscosity (η_a) was then given by

$$\eta_a = \frac{\tau_w}{\dot{\gamma}_w} \quad (4)$$

For a fluid that obeys a rheological power law, the shear stress is proportional to the shear rate

$$\tau_w = K(\dot{\gamma}_w)^n \quad (5)$$

where K is the limiting zero-shear (Newtonian) viscosity and n is the power law index. Substituting equation (4) into equation (5) gives

$$\eta_a = K(\dot{\gamma}_w)^{n-1} \quad (6)$$

or expanding

$$\log \eta_a = \log K + (n-1)\log \dot{\gamma}_w \quad (7)$$

The slope of the plot of log viscosity vs log shear rate in the range where equation (5) applies represents the value of $n-1$. Newtonian behaviour corresponds to $n = 1$, and shear-thinning (pseudoplastic) behaviour to $n < 1$. The power law index in the present study was calculated over the shear rate region of 133–1333 s^{-1} where a reasonably straight line could be drawn through the data in most instances.

RESULTS AND DISCUSSION

Melt rheology

The melt viscosities of PET and SEBS-g-MA at 260°C and 280°C are plotted as a function of shear rate in *Figure 1a*. The melt viscosity of PET was higher than that of SEBS-g-MA, and it decreased less rapidly with shear rate. This is reflected in lower values of the power law index (n) calculated from the three highest shear rates (*Table 1*). The power law index increased with temperature for both PET and SEBS-g-MA. The magnitude of n for PET, and the increase in n with increasing temperature, were consistent with previously published results ($n = 0.82$ at 280°C and $n = 0.88$ at 325°C)[23]. The trend from pseudoplastic toward Newtonian behaviour at higher temperatures is generally attributed to

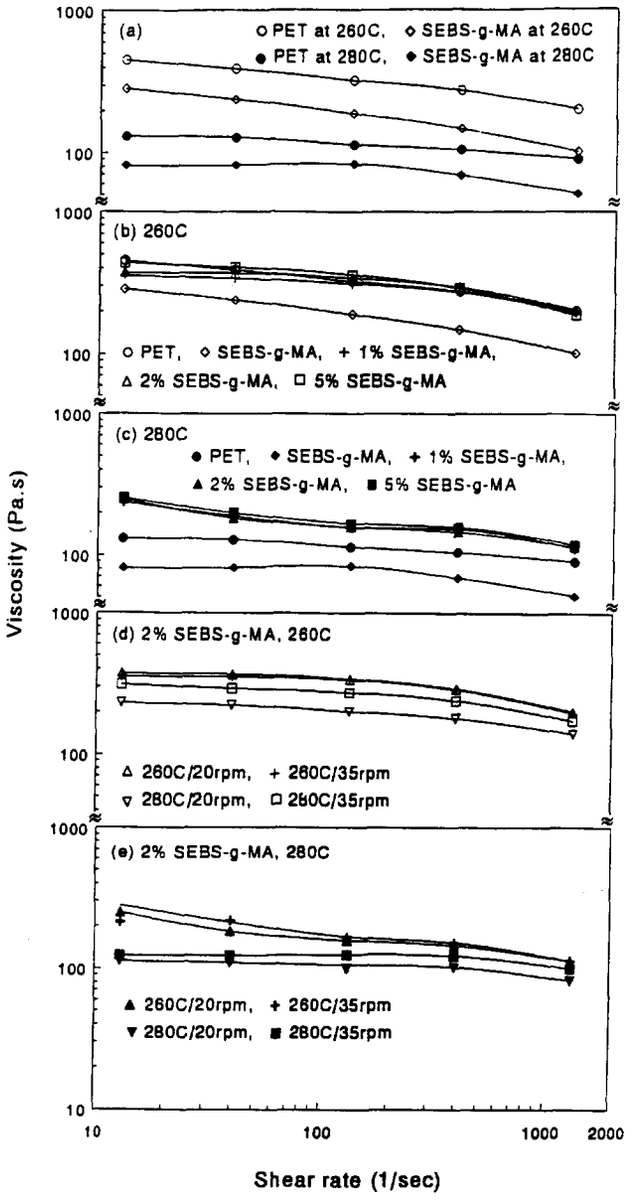

Figure 1 Melt viscosity. (a) Extruded PET and SEBS-g-MA at 260 and 280°C; (b) effect of composition at 260°C (blends processed at 260°C/20 rpm); (c) effect of composition at 280°C (blends processed at 260°C/20 rpm); (d) effect of processing variables on the 2% SEBS-g-MA blend at 260°C; and (e) effect of processing variables on the 2% SEBS-g-MA blend at 280°C

Table 1 Rheological properties of PET and SEBS-g-MA blends

Material	Processing conditions	M_n	n 260°C	n 280°C
PET	As received	24 000	0.74	0.88
	280°C/35 rpm	21 000	0.79	0.89
SEBS-g-MA	As received	74 000	0.72	0.78
1% SEBS-g-MA	260°C/20 rpm	21 000	0.79	0.85
2% SEBS-g-MA		21 000	0.77	0.85
5% SEBS-g-MA		22 000	0.71	0.85
2% SEBS-g-MA	260°C/35 rpm	22 000	0.76	0.83
	280°C/20 rpm	18 000	0.84	0.91
	280°C/35 rpm	21 000	0.80	0.90

increased Brownian motion which makes alignment of the molecules more difficult.

The effect of SEBS-g-MA on the melt viscosity of blends processed at 260°C/20 rpm is shown in *Figures 1b* and *c*. Data from processed PET, which had a molecular weight comparable to that of PET in the blends, are included for comparison. Addition of up to 5% SEBS-g-MA had very little effect on the melt viscosity of PET at 260°C. Subtle differences in the shear rate dependence were responsible for the slight decrease in the power law index with increasing SEBS-g-MA content. At 280°C, the viscosity and the power law index of the blends were independent of the SEBS-g-MA content. At this temperature, blending with SEBS-g-MA increased the viscosity of PET. This 'positive-deviation' behaviour, where mixing two polymers results in an increase in viscosity above the values of the two pure components, is often observed when a thermoplastic is blended with an elastomer[24].

Blends with 2% SEBS-g-MA were used to examine the effect of processing conditions. Increasing the blending temperature from 260°C to 280°C produced a blend with lower viscosity and higher power law index. In contrast, the screw speed had virtually no effect on either the viscosity or the power law index of blends processed at 260°C (*Figure 1d*). Although screw speed appeared to affect the viscosity of the blends processed at 280°C, the lower molecular weight of the 280°C/20 rpm blend could account for this difference. The large drop in molecular weight for this processing condition probably resulted from the combination of long residence time and high temperature.

Blend characterization

Blends of PET with functionalized SEBS-g-MA and unfunctionalized SEBS were extracted in an attempt to isolate an SEBS-g-MA component that had chemically reacted with PET. The C–H stretching region at 3000–2800 cm^{-1} was used to identify PET and SEBS in the fractions. The PET had relatively weak absorbances in this region at 2907 and 2969 cm^{-1}. Considerably stronger absorbances at 2852, 2923 and 2959 cm^{-1} characterized SEBS and SEBS-g-MA. The THF-soluble fractions from the two blends contained the same amount of material, about 16%. Spectra of these THF-soluble fractions exhibited only absorbances of SEBS in the 3000–2800 cm^{-1} region. The THF-insoluble fraction from the blend of the unfunctionalized SEBS with PET exhibited only absorbances of PET, indicating that complete separation of the phases was achieved. The C–H stretching region of the THF-insoluble fraction from the blend of SEBS-g-MA with PET is compared with spectra of the blend components in *Figure 2*. The spectrum of the fraction exhibits overlapping absorbances of PET at 2907 and 2969 cm^{-1} and SEBS at 2852, 2923 and 2959 cm^{-1}. Although most of the SEBS-g-MA was extracted with THF, and therefore had not reacted with PET, the small amount that reacted was easily detected in the THF-insoluble fraction by the strong absorbances of SEBS in the C–H stretching region.

Blend morphology

Figure 3 presents an etched surface of the 5% SEBS-g-MA blend. The holes that remained after the SEBS-g-MA phase was removed by etching reveal the size of the spherical SEBS-g-MA particles. The particle size distribution (0.1–1.0 μm) and the average particle size (0.33 μm for 1% and 2% SEBS-g-MA blends and 0.37 μm for the 5% SEBS-g-MA blend) were essentially independent of SEBS-g-MA content (*Table 2*). The absence of a strong dependency of particle size on composition is characteristic of reactive blends. In

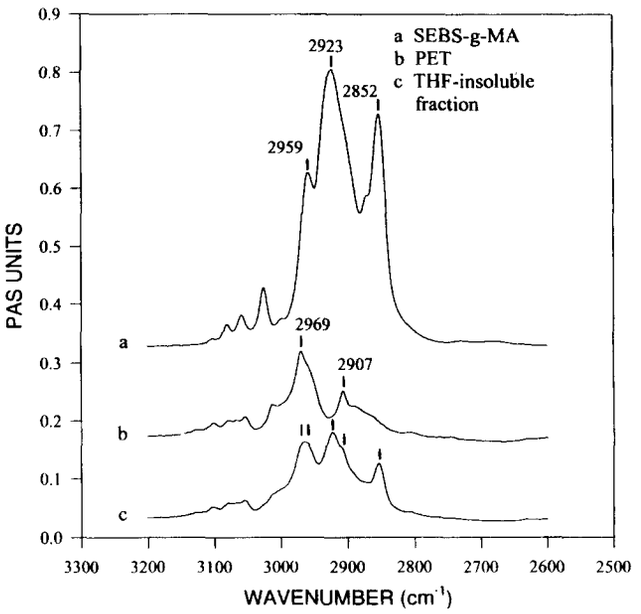

Figure 2 The 3000–2800 cm^{-1} region in the photoacoustic *FT*i.r. spectra of: (a) SEBS-g-MA, (b) PET, and (c) the THF-insoluble fraction of the 25% SEBS-g-MA blend

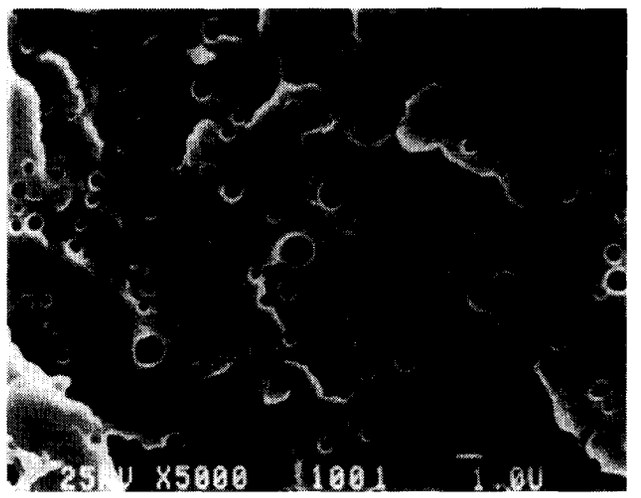

Figure 3 Scanning electron micrograph of an etched surface of the 5% SEBS-g-MA blend

Table 2 Particle size and hydroxyl/anhydride ratio of SEBS-g-MA blends

Material	Processing conditions	D^a (μm)	R^b
1% SEBS-g-MA	260°C/20 rpm	0.33 ± 0.12	28.9
2% SEBS-g-MA		0.33 ± 0.16	14.3
5% SEBS-g-MA		0.37 ± 0.17	5.5
2% SEBS-g-MA	260°C/35 rpm	0.40 ± 0.12	14.3
	280°C/20 rpm	0.45 ± 0.14	14.3
	280°C/35 rpm	0.39 ± 0.12	14.3

[a] D = average SEBS-g-MA particle diameter
[b] R = hydroxyl/anhydride ratio

addition, the particle size was not very sensitive to processing conditions, a feature that has been observed with other reactive blends[25,26]. It is generally believed that the graft copolymer formed *in situ* acts as an emulsifier to decrease the interfacial tension and reduce the tendency of dispersed particles to coalesce with increasing volume fraction. The THF-extractability of a significant fraction of the SEBS-g-MA indicated that the most likely model of an elastomer particle was a core of ungrafted SEBS-g-MA surrounded by the graft copolymer. The amount of grafting did not appear to be limited by the availability of hydroxyl groups, as

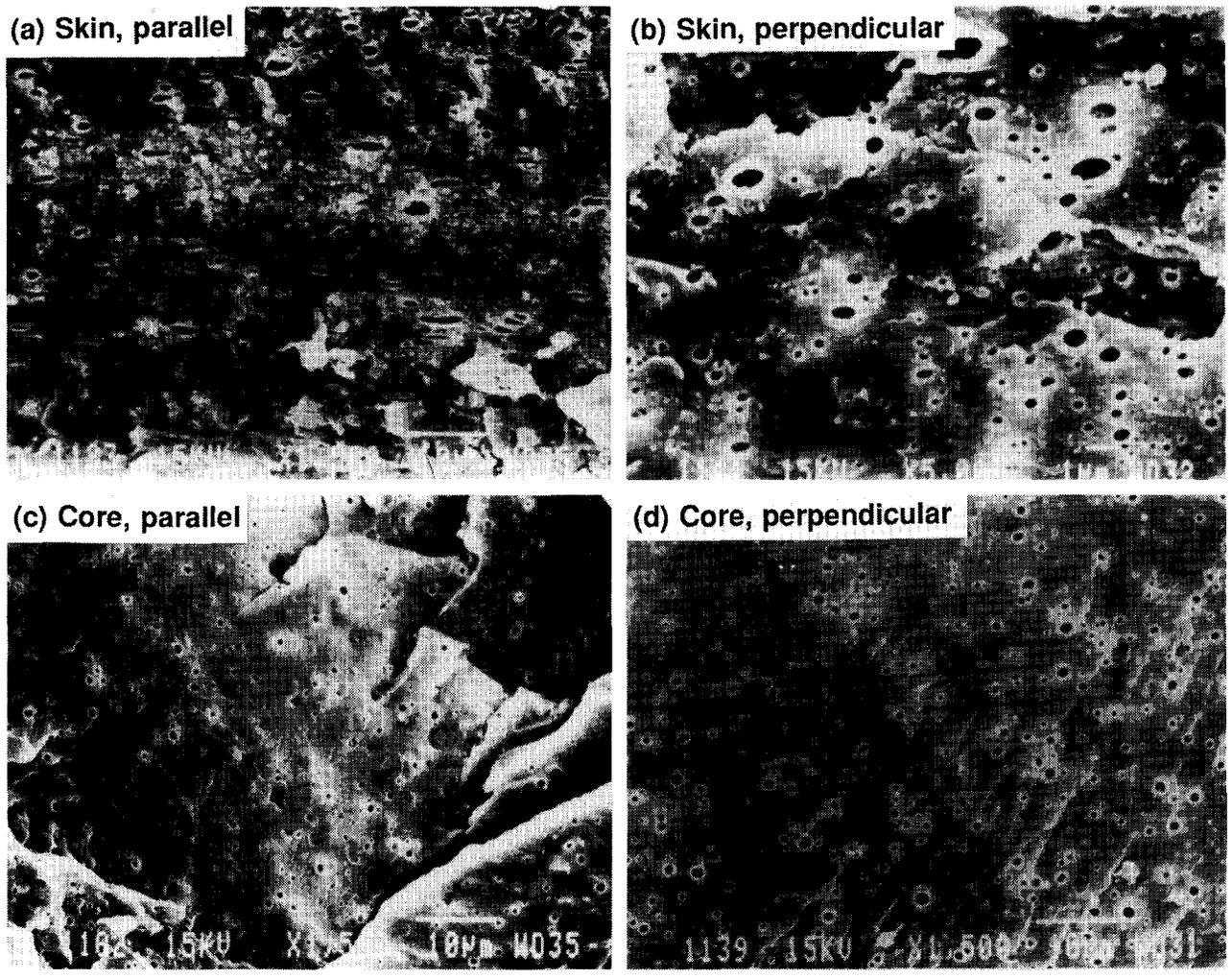

Figure 4 Scanning electron micrographs of freeze-fractured and etched surfaces from an injection moulded tensile specimen of the 2% SEBS-g-MA blend (260°C/20 rpm). (a) Parallel to the injection direction near the edge; (b) perpendicular to the injection direction near the edge; (c) parallel to the injection direction near the centre; (d) perpendicular to the injection direction near the centre; and (e) schematic of the skin-core morphology

the PET hydroxyl number exceeded the total anhydride content of the SEBS-g-MA phase (*Table 2*). More likely, the amount of graft copolymer was determined by the extent of interfacial contact between the two phases.

Characterization of injection moulded specimens

Injection moulded specimens of all the blends exhibited a skin-core morphology. The micrographs in *Figure 4* show the edge and the centre of an injection moulded specimen with 2% SEBS-g-MA (260°C/20 rpm) that was freeze-fractured parallel and perpendicular to the injection direction and then etched to remove the SEBS-g-MA phase. The holes near the edge of the parallel fracture surface contained SEBS-g-MA domains less than 1 μm in diameter that were elongated in the injection direction (*Figure 4a*). Perpendicular to the injection direction, *Figure 4b*, circular holes near the edge indicated that the elongated SEBS-g-MA domains were predominantly rod-shaped. A few of the holes were oval suggesting that some of the elongated SEBS-g-MA domains were slightly flattened. The elongated domains extended only about 100 μm inward from the edge. Through the remainder of the thickness, the domains were spherical and on the order of 1 μm in diameter (*Figures 4c* and *d*). All the injection moulded blends exhibited the skin-core morphology shown schematically in *Figure 4e*.

Heating and cooling thermograms of injection moulded PET and the blend with 2% SEBS-g-MA (260°C/20 rpm) are compared in *Figure 5*. These specimens, taken from the centre of injection moulded tensile bars, were almost amorphous as indicated by the well defined glass transition at about 70°C and the large cold crystallization exotherm near 130°C (*Figure 5a*). As is often the case when a second component is added to PET, SEBS-g-MA acted as a nucleating agent by shifting the cold crystallization temperature (T_{cc}) of PET approximately 10°C lower (*Table 3*). However the temperature, enthalpy and shape of the subsequent melting endotherm were not affected by the presence of SEBS-g-MA. The difference between the heat of melting and the heat of cold crystallization represented the amount of crystallinity in the as-moulded tensile bar. This was about 12% for PET and slightly higher, in the range of 15%, for the blends. The SEBS-g-MA also nucleated crystallization from the melt by shifting the crystallization temperature (T_c) slightly higher and narrowing the crystallization peak (*Figure 5b*). Molecular weight can conceivably affect T_{cc} and T_c. Although the injection moulding process resulted in molecular weight reduction for both PET and the blend, the final molecular weights were not significantly different [M_n = 17 000 for PET and M_n = 18 000 for 2% SEBS-g-MA (260°C, 20 rpm)].

Tensile properties

Tensile deformation of PET and all the blends was accompanied by necking and cold drawing. Typical stress–strain behaviour of the most ductile materials is illustrated schematically in *Figure 6*. A macro-shearband formed at the yield point (σ_y) and a neck subsequently propagated sequentially first from one side of the macro-shearband and then from the other side. The engineering stress dropped to about half the yield stress as the neck started to propagate from one side of the macro-shearband; cold drawing at a constant engineering stress continued until the neck reached the end of the gauge section (cold drawing I). The corresponding engineering strain (ε_1) depended upon the length of the gauge section between the initial macro-shearband and the gripping tab. After the neck reached the end of the

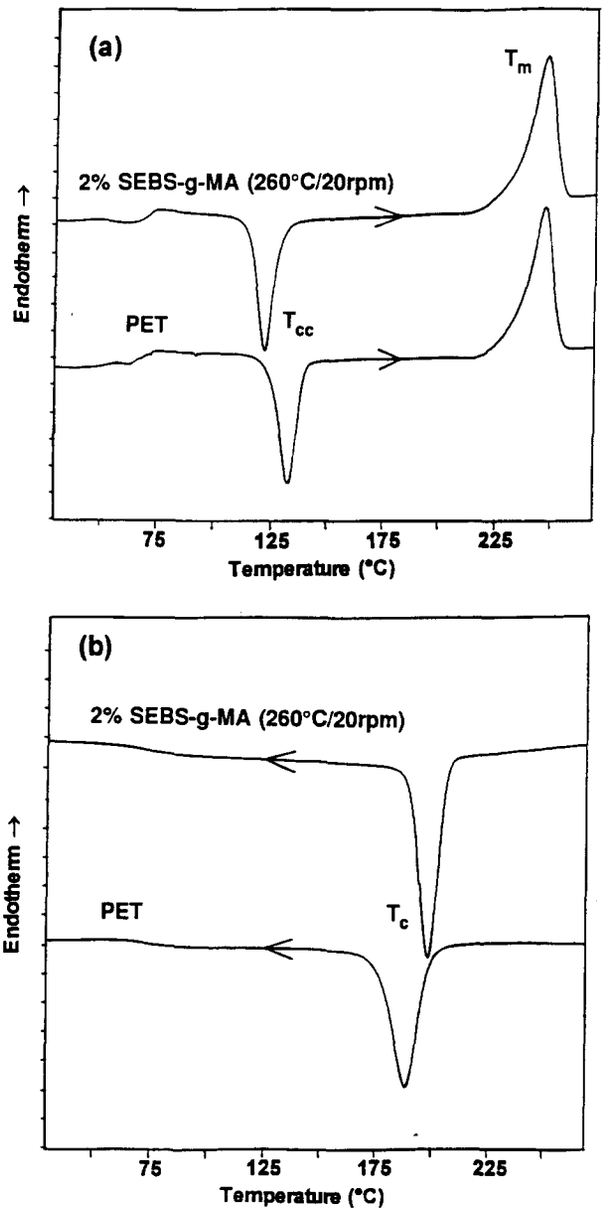

Figure 5 Heating and cooling thermograms of injection moulded PET (as received) and the blend with 2% SEBS-g-MA (260°C/20 rpm)

Table 3 Thermal properties of PET and SEBS-g-MA blends

Material	T_{cc} (°C)	ΔH_{cc}^a (J g^{-1})	T_m (°C)	ΔH_m (J g^{-1})	X^b (%)	T_c (°C)	ΔH_c (J g^{-1})
PET[c]	133	30	247	44	12	189	44
1% SEBS-g-MA[d]	126	26	245	43	14	191	42
2% SEBS-g-MA[d]	122	28	247	47	15	198	46
5% SEBS-g-MA[d]	121	27	248	46	15	195	44

[a] Per gram of PET
[b] Initial crystallinity using 122 J g^{-1} as the heat of fusion of PET
[c] As received
[d] Processed at 260°C/20 rpm

gauge section, the necked region uniformly strain hardened with gradually increasing stress and simultaneously the neck continued to propagate a short distance into the wider gripping tab (strain hardening I). When the engineering stress increased sufficiently, cold drawing initiated at the other side of the macro-shearband, accompanied by another stress drop, and continued at constant stress to the other end of the gauge section (cold drawing II). A second region of uniform strain hardening started when the entire gauge section had necked, and continued until the specimen fractured at one end of the neck (strain hardening II). The relative magnitudes of the engineering strains ε_1 and ε_2 for sequential neck propagation depended on the position of the initial macro-shearband in the gauge section.

The effect of SEBS-g-MA content on the yield stress was consistent with the rule of mixtures (*Table 4*). A macro-shearband formed at the yield point for PET and all the blends, however some of the compositions fractured before the sequential cold drawing process was complete. Typically PET fractured at the end of the neck after the neck had propagated only a short distance (*Figure 7a*). In all the blends processed at 260°C/20 rpm, the neck propagated from one side of the macro-shearband all the way to the end of the gauge section, then fractured at the end of the neck after strain hardening (*Figure 7a*). The portion of the gauge section on the other side of the macro-shearband remained undrawn when these specimens fractured. Because the elongation at break depended on the length of the cold drawn gauge section, the values reported in *Table 4* for the blends processed at 260°C/20 rpm have a large standard deviation. For the same reason, the apparent increase in the elongation at break with increasing SEBS-g-MA content may be misleading.

The blend processed at 280°C/20 rpm also fractured at the end of the first cold drawing region (*Figure 7b*). In contrast, the two blends processed at 35 rpm (260°C/35 rpm and 280°C/35 rpm) did not fracture after the first cold drawing and strain hardening regions, instead the neck started to propagate from the other side of the macro-shearband as the stress dropped to a second cold drawing region of constant stress (*Figure 7b*). After the neck reached the other end of the gauge section, there was a second strain hardening region that terminated when the specimen fractured at the end of the neck. There was much less variability in the elongation at break when the entire gauge section necked before fracture (*Table 4*).

When the strain rate was increased from 100% min^{-1} to 1000% min^{-1}, the yield stress increased and the fracture strain decreased (*Table 4*). All the materials

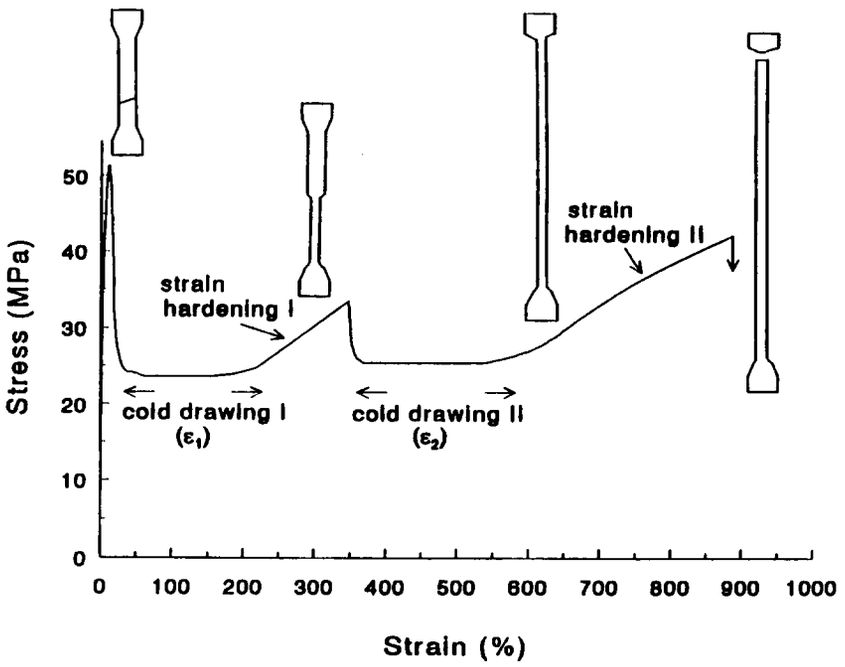

Figure 6 Schematic of the stress–strain curve showing the two cold drawing and the two strain hardening regions of the most ductile samples

Table 4 Yield stress and elongation at break of PET and SEBS-g-MA blends

Material	Processing condition	σ_y (MPa) $\dot{\varepsilon} = 100\%\ min^{-1}$	σ_y (MPa) $\dot{\varepsilon} = 1000\%\ min^{-1}$	ε_b (%) $\dot{\varepsilon} = 100\%\ min^{-1}$	ε_b (%) $\dot{\varepsilon} = 1000\%\ min^{-1}$
PET	As received	55.1 ± 0.4	66.4 ± 0.3	77 ± 13	19 ± 3
1% SEBS-g-MA	260°C/20 rpm	54.5 ± 0.3	n/a	403 ± 166	n/a
2% SEBS-g-MA		52.3 ± 1.3	61.1 ± 2.4	462 ± 186	43 ± 12
5% SEBS-g-MA		48.7 ± 1.3	57.3 ± 1.6	637 ± 105	69 ± 19
2% SEBS-g-MA	260°C/35 rpm	50.9 ± 0.4	62.1 ± 0.4	816 ± 54	90 ± 42
	280°C/20 rpm	51.3 ± 1.0	61.5 ± 0.3	335 ± 79	22 ± 16
	280°C/35 rpm	51.5 ± 0.4	61.1 ± 0.3	869 ± 56	162 ± 49

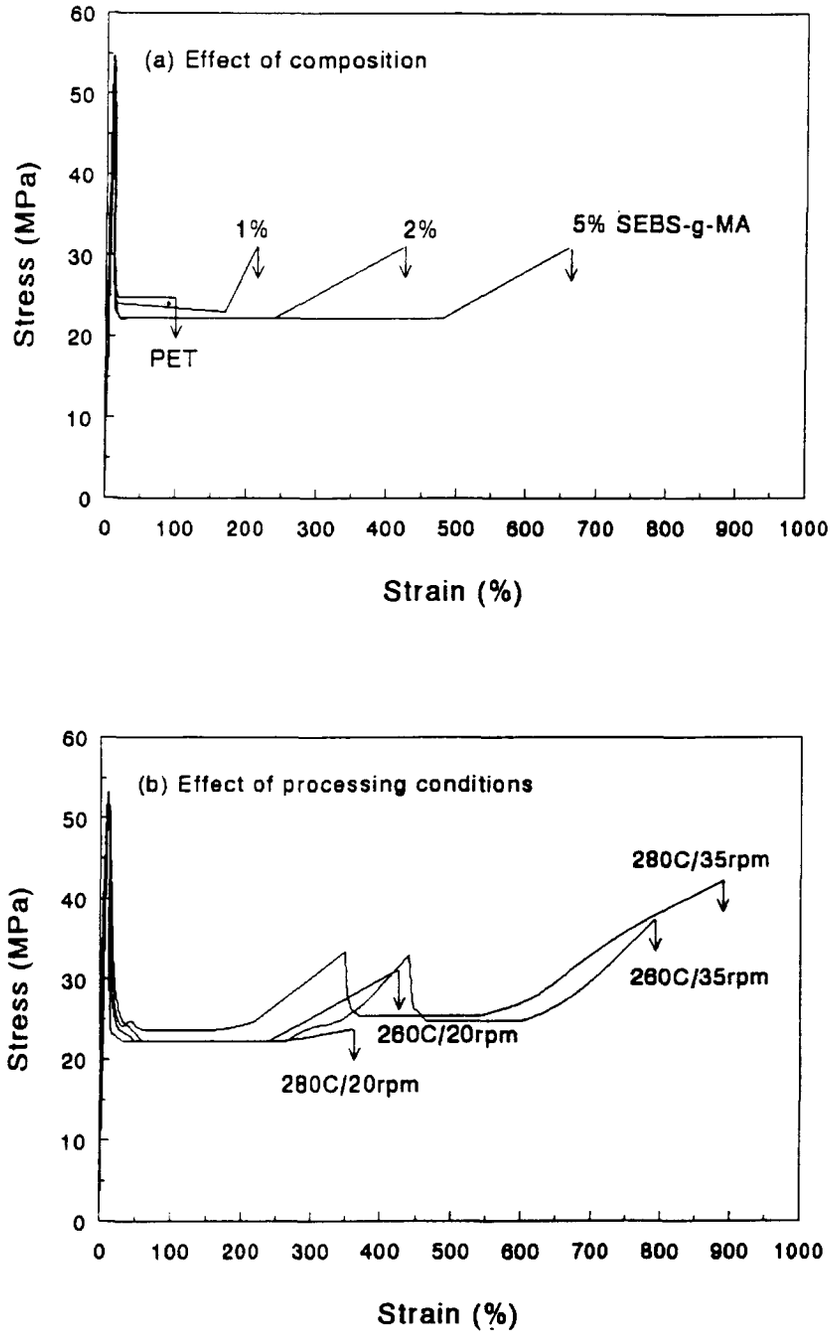

Figure 7 Stress–strain curves with a strain rate of 100% min $^{-1}$. (a) Effect of composition for blends processed at 260°C/20 rpm; and (b) effect of processing variables on blends with 2% SEBS-g-MA

yielded with formation of a macro-shearband, then fractured in the first cold drawing region before the propagating neck reached the end of the gauge section (*Figure 8*). The site of fracture was the propagating end of the neck. The fracture strain measured the distance the neck propagated before fracture, and thus indicated the relative stability of the neck. The increase in fracture strain with increasing SEBS-g-MA content, and the higher fracture strain of the two blends processed at the higher screw speed, confirmed trends suggested by the lower strain rate data.

It is the ability of polymers like PET to strain-harden that makes possible the development of a stable neck. Once stabilized, the neck propagates along the gauge section in the process known as cold drawing. In PET, the stability and strength of the propagating neck depend on orientation and strain-induced crystallization. The extent of strain crystallization, as indicated by the heat of melting of the drawn material in the neck, was the same for PET and all the blends, about 54 J g^{-1}, which corresponded to a crystallinity of 44%. Nevertheless, blending with SEBS-g-MA clearly enhanced the strength and stability of the propagating neck. Several factors may have contributed. It is not unusual for the temperature in the propagating neck to approach or even exceed the glass transition of PET. In the present study, temperatures in the range of 80°C were typically measured with an i.r. temperature sensor. To prevent softening and failure in the neck, it is essential that strengthening mechanisms occur rapidly. It has been suggested that the rates of crystallization and orientation during cold drawing are increased by a second phase[27].

Because SEBS-g-MA was found to nucleate cold crystallization and crystallization from the melt, it is proposed that it also accelerated strain crystallization.

Cavitation could also have contributed to the enhanced stability of the propagating neck in the SEBS-g-MA blends. The entire neck of the blends was profusely stress-whitened; in comparison, the neck of the PET control was clear with some stress-whitening only in the immediate region of the fracture site. The morphology in the neck of an SEBS-g-MA blend consisted of a network of fine fibrils with profuse voiding (*Figure 9a*). In comparison, the fibrils near the fracture site of PET were much thicker (*Figure 9b*), and the origin of stress-whitening appeared to be fibril splitting rather than formation and growth of voids. Although the stress state in tensile testing is generally considered to be uniaxial tension, the shape of the neck produces a triaxial component[28]. It is likely that cavitation of SEBS-g-MA particles relieved triaxiality in the blends, thereby enabling the PET matrix to neck under a less severe stress state.

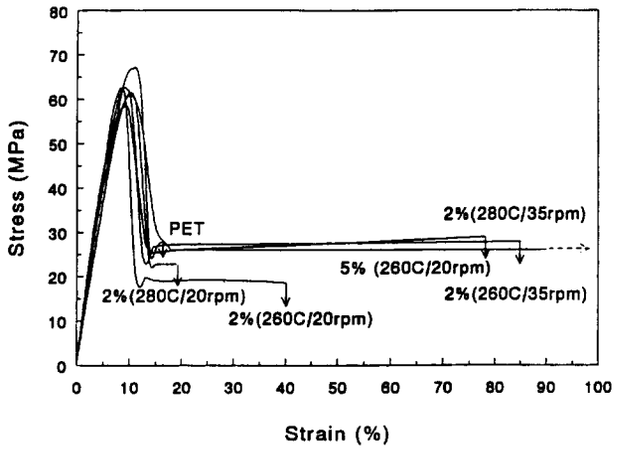

Figure 8 Stress–strain curves with a strain rate of 1000% min^{-1}

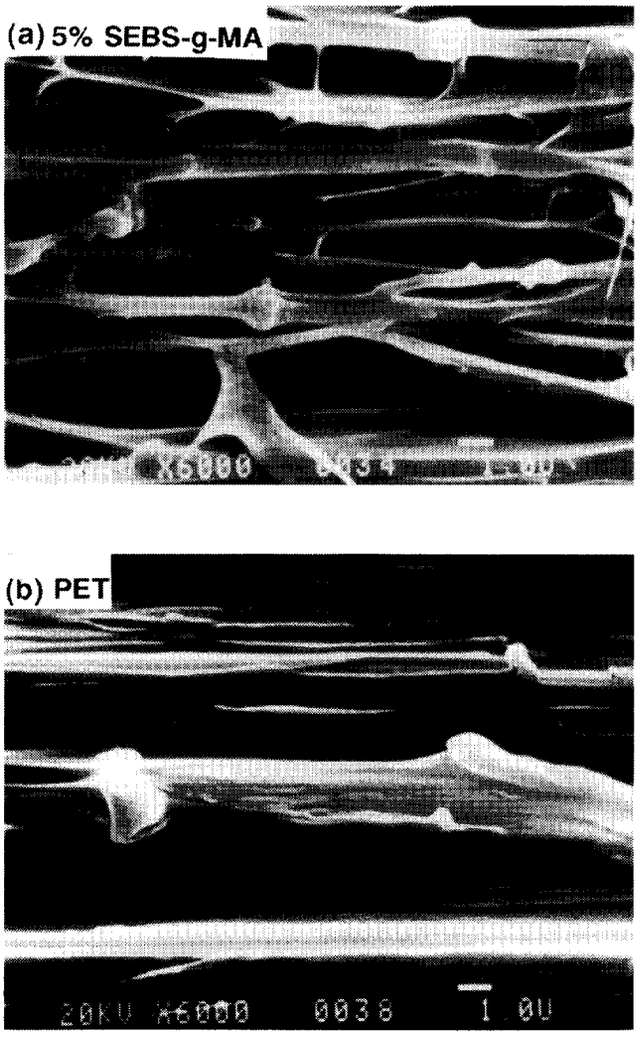

Figure 9 Scanning electron micrographs of the necked region cryogenically fractured parallel to the tensile direction. (a) Blend with 5% SEBS-g-MA; and (b) PET

In summary, as little as 1% of SEBS-g-MA in PET increased the elongation at break by more than a factor of 10. The observations were consistent with *in situ* formation of a graft copolymer by reaction of PET hydroxyl end groups with maleic anhydride. In the melt, the graft copolymer acted as an emulsifier to decrease the interfacial tension and reduce the tendency of dispersed particles to coalesce. In the solid state, the graft copolymer promoted adhesion between the phases in the blend and facilitated cavitation in a triaxial stress state. In addition, the dispersed particles acted as a nucleating agent to enhance crystallization during yielding. Although the degree of strain-induced crystallization was unaffected, it is suggested that the increased rate of crystallization and orientation stabilized the propagating neck.

ACKNOWLEDGEMENT

The generous financial support of the Shell Chemical Company is gratefully acknowledged.

REFERENCES

1 Gelles, R., Modic, M. and Kirkpatrick, J. *SPE ANTEC Tech. Papers* 1988, **34**, 513
2 Cheng, C., Peduto, N., Hiltner, A., Baer, E., Soskey, P. R. and Mylonakis, S. G. *J. Appl. Polym. Sci.* 1994, **53**, 513
3 Nishimoto, M., Keskkula, H. and Paul, D. R. *Polymer* 1991, **32**, 272
4 Cheng, C., Hiltner, A., Baer, E., Soskey, P. R. and Mylonakis, S. G. *J. Appl. Polym. Sci.* 1994, **52**, 177
5 Cheng, C., Hiltner, A., Baer, E., Soskey, P. R. and Mylonakis, S. G. *J. Mater. Sci.* 1995, **30**, 587
6 Hourston, D. J., and Lane, S. in 'Rubber Toughened Engineering Plastics' (Ed. A. A. Collyer), Chapman & Hall, London, 1994, p. 243
7 Brady, A. J., Keskkula, H. and Paul, D. R. *Polymer* 1994, **35**, 3665
8 Majumdar, B., Keskkula, H. and Paul, D. R. *J. Appl. Polym. Sci.* 1994, **54**, 339
9 Cecere, A., Greco, R., Ragosta, G., Scarinzi, G. and Taglialatela, A. *Polymer* 1990, **31**, 1239
10 Di Liello, V., Laurienzo, P., Malinconico, M., Martuscelli, E., Ragosta, G. and Volpe, M. G. *Angew. Makromol. Chem.* 1990, **174**, 141
11 Hourston, D. J., Lane, S., Zhang, H. X., Bootsma, J. P. C. and Koetsier, D. W. *Polymer* 1991, **32**, 1140
12 Penco, M., Pastorino, M. A., Occhiello, E., Garbassi, F., Braglia, R. and Giannotta, G. *J. Appl. Polym. Sci.* 1995, **57**, 329
13 Gilmore, D., Kirkpatrick, J., and Modic, M. J. *SPE ANTEC Tech. Papers* 1990, **36**, 1228
14 Modic, M. J. and Pottick, L. A. *Polym. Eng. Sci.* 1993, **33**, 819
15 Oshinski, A. J., Keskkula, H. and Paul, D. R. *Polymer* 1992, **33**, 268

16 Oshinski, A. J., Keskkula, H. and Paul, D. R. *Polymer* 1992, **33**, 284
17 Majumdar, B., Keskkula, H. and Paul, D. R. *Polymer* 1994, **35**, 1386
18 Majumdar, B., Keskkula, H. and Paul, D. R. *Polymer* 1994, **35**, 1399
19 van der Sanden, M. C. M. and Meijer, H. E. H. *Polymer* 1994, **35**, 2774
20 Moore, Jr., L. D. *ACS Polymer Preprints* 1960, **1 (1)**, 234
21 Smith, C. W. and Dole, M. *J. Polym. Sci.* 1956, **20**, 37
22 Roberts, R. C. *Polymer* 1969, **10**, 113
23 Wu, S. *Polym. Eng. Sci.* 1987, **27**, 335
24 Utracki, L. A. and Kamal, M. R. *Polym. Eng. Sci.* 1982, **22**, 96
25 Willis, J. M., Favis, B. D. and Lunt, J. *Polym. Eng. Sci.* 1990, **30**, 1073
26 Willis, J. M., Caldas, V. and Favis, B. D. *J. Mater. Sci.* 1991, **26**, 4742
27 Wilfong, D. L., Hiltner, A. and Baer, E. *J. Mater. Sci.* 1986, **21**, 2014
28 G'Sell, C., Aly-Helal, H. A. and Jones, J. J. *J. Mater. Sci.* 1983, **18**, 1731